Electronic Supplementary Information (ESI)

Nitrogen-doped Graphene-Supported Cobalt Carbonitride@Oxide Core-Shell Nanoparticles as a Non-noble Metal Electrocatalyst for Oxygen Reduction Reaction

Yingsi Wu, Qianqian Shi, Yuhang Li, Zhuangchai Lai, Hao Yu*, Hongjuan Wang, Feng Peng*

School of Chemistry and Chemical Engineering, South China University of Technology, Guangzhou, 510640, China. Email: yuhao@scut.edu.cn (H.Y.); cefpeng@scut.edu.cn (F.P.); Tel. & Fax.: +86-20-8711 4916.

1. Calculations for K-L plots and Tafel plots

To investigate the kinetics of the catalysts in ORR, LSV curves performed at various rotating speeds and the Koutecky-Levich (K-L) plots (J^{-1} vs. $\omega^{-1/2}$) were obtained. RDE measurements on the $CoCN@CoO_x(18)$/NG and h-Co_3O_4/NG catalysts show the current densities increased with the rotating speeds increased from 400 to 2800 rpm (Fig. 4b, c). According to the K-L theory, the inverse of current density (J^{-1}) is plotted against the inverse of the square root of the rotating speed ($\omega^{-1/2}$) at different potential values (inserts of Fig. 4b, c). The transferred electron number (n) per oxygen molecule involved in the ORR process can be calculated from the slope of the K-L plots using the following equation:

$J^{-1} = J_L^{-1} + J_K^{-1} = (0.62nFCD^{2/3}\nu^{-1/6}\omega^{1/2})^{-1} + J_K^{-1}$,

where J is the measured current density, J_L is the diffusion limiting current density, J_K is the kinetic current density. n is the overall number of electrons transferred in ORR, F is the Faraday constant (F = 96485 C mol^{-1}), C is the concentration of O_2, D is the diffusion coefficient of O_2, ν is the kinematic viscosity of the electrolyte, and ω is the electrode rotating speed in rpm. Since in our study the electrolyte was the O_2-saturated 0.1 M KOH solution, the values C, D and ν were used as 1.2×10^{-3} M, 1.9×10^{-5} cm^2 s^{-1} and 0.01 cm^2 s^{-1}, respectively.

For Tafel plots, the kinetic current density was calculated from the relation in K-L equation:

$$J_K = \frac{J \times J_L}{(J_L - J)}$$

From K-L equation, the diffusion limiting current density J_L of $CoCN@CoO_x(18)/NG$ is calculated as 5.33 mA cm^{-2}, which is close to that of Pt-C (5.70 mA cm^{-2}) and higher than that of h-Co_3O_4/NG (4.82 mA cm^{-2}).

2. Supplementary results

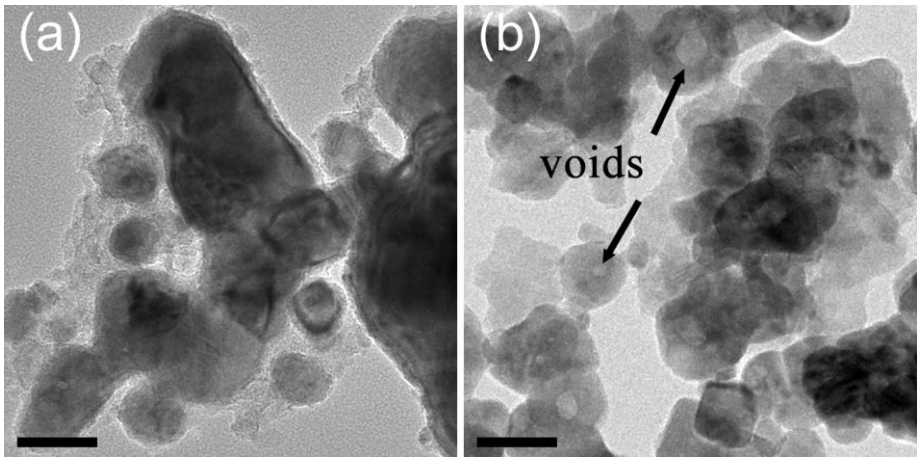

Fig. S1 TEM images of bulk (a) CoN and (b) Co_3O_4 samples. Scale bars: 50 nm.

The oxidation of bulk CoN without NG resulted in solid Co_3O_4 particles, although some hollow structures can be observed, as shown in Fig. S1, due to the longer diffusion distance in the larger particles.[1]

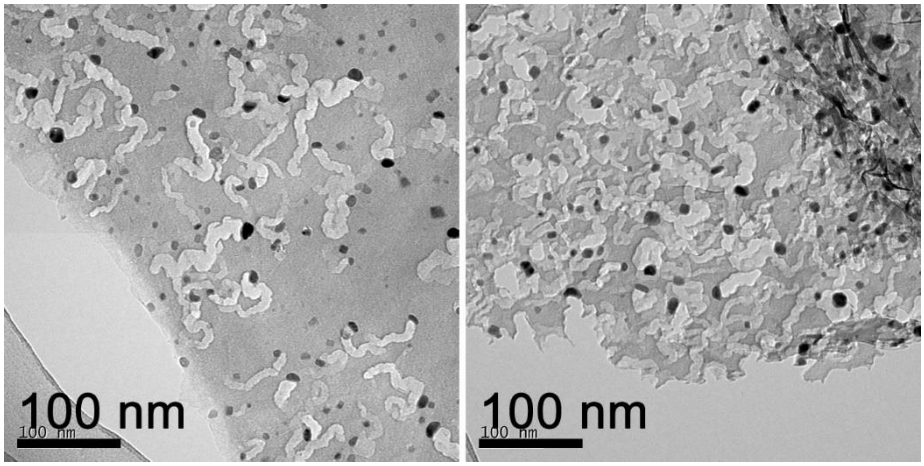

Fig. S2 TEM images of $CoCN@CoO_x/NG$.

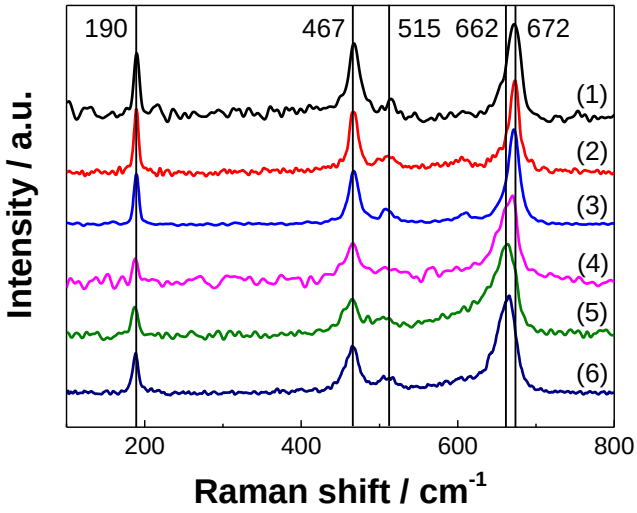

Fig. S3 Raman spectra of (1) CoCN@CoO_x(18)/NG, (2) CoCN@CoO_x(63)/NG, (3) CoN, (4) h-Co_3O_4/NG, (5) CoO and (6) Co_3O_4.

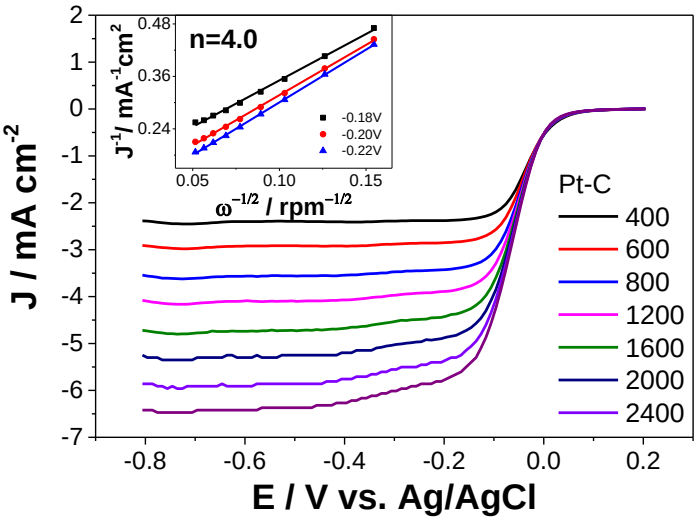

Fig. S4 LSV curves of Pt-C at various rotating speeds with a scan rate of 10 mV/s in O_2-saturated 0.1 M KOH solution; the inset is the calculated K–L plots at different potentials (-0.18, -0.20, -0.22 V vs. Ag/AgCl).

Synthesis and characterizations of CoCN@CoO_x/NG with different particles sizes

Three deposition methods have been applied to control the size of CoCN@CoO_x particles on graphene: homogeneous oxidative precipitation (HP), NH_3·H_2O-catalyzed hydrolysis (N) and the direct impregnation of acetate cobalt (I). Fig. S5 show the TEM images and size distributions of the CoCN NPs prepared from these three methods. The particle size of CoCN@CoO_x(5)/NG is relatively larger than the other two samples. The more detailed statistic on the NPs shows their shell thickness and core diameters, as listed in Table S4 and represented by the TEM images in Fig. S6.

As shown in Table S4, the shell thickness remains unchanged across the three

samples, therefore the volume ratio (V_{core}/V_{shell}) grows with the particle size. It was also noted that, since the smaller particles are more prone to be oxidized to form hollow structures, the percentage of hollow NPs decreased from 25.7% to 6.5% with the particle size increasing.

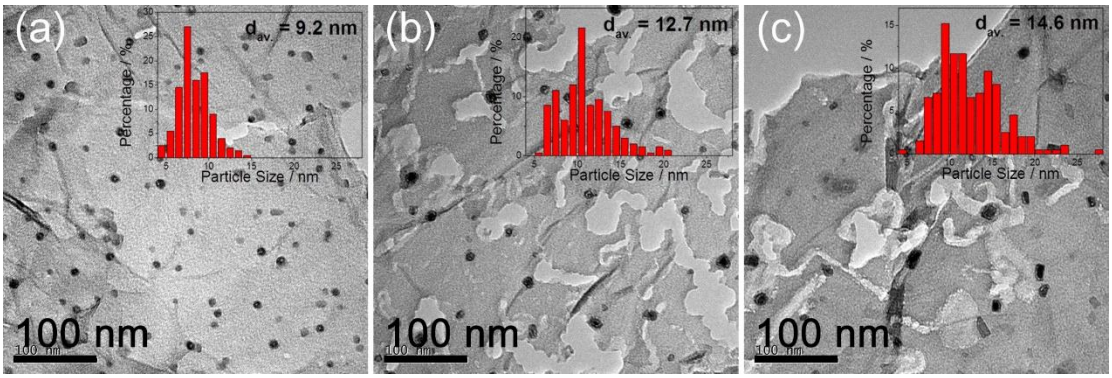

Fig. S5 TEM images of (a) CoCN@CoO_x/NG-HP, (b) CoCN@CoO_x/NG-I and (c) CoCN@CoO_x(5)/NG.

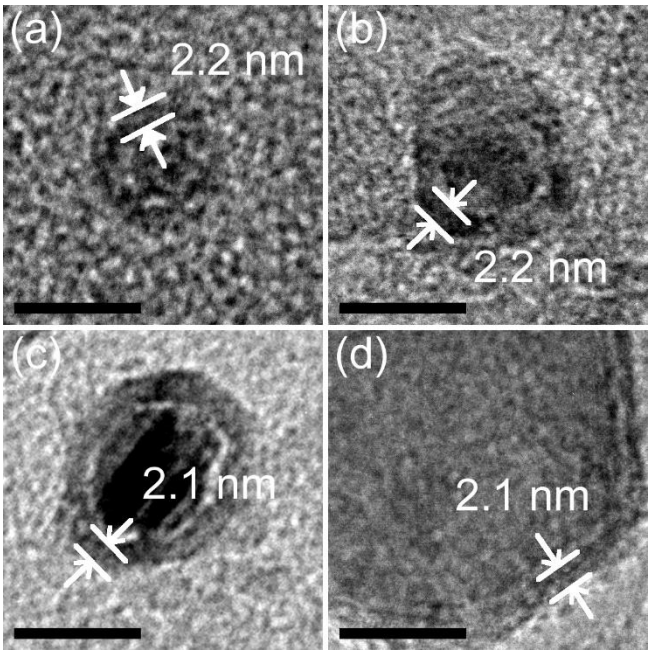

Fig. S6 HRTEM images of (a) CoCN@CoO_x/NG-HP, (b) CoCN@CoO_x/NG-I, (c) CoCN@CoO_x(5)/NG and (d) CoCN@CoO_x(18)/NG. Scale bars: 10 nm.

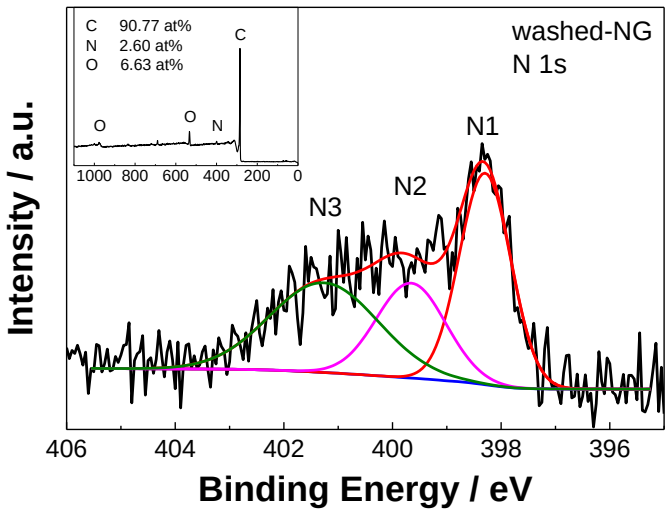

Fig. S7 XPS survey and high resolution N 1s spectrum of washed NG. The O content of 6.63at% in the survey spectrum may be from the oxygen-containing groups on GO, which cannot be completely removed by NH_3 annealing at 700 ^oC, depositing CoCN particles and subsequent HCl washing.

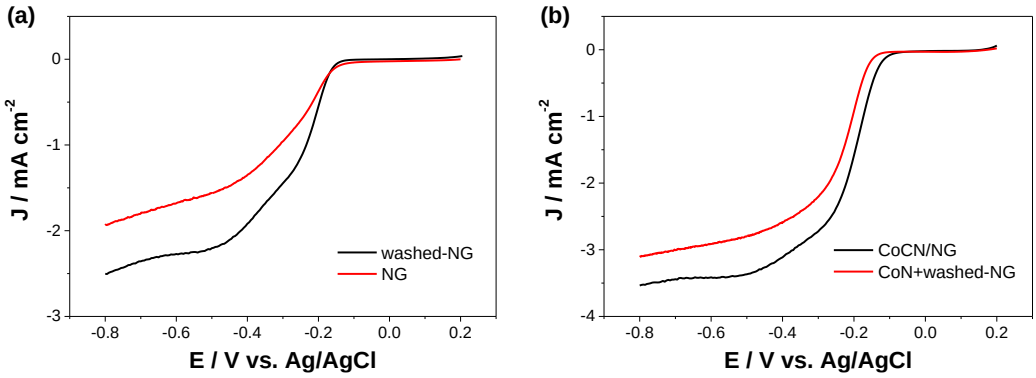

Fig. S8 LSV curves of (a) washed-NG and NG, (b) CoCN/NG and CoN+washed-NG in O_2-saturated 0.1 M KOH solution at 1600 rpm rotating speed with a scan rate of 10 mV/s.

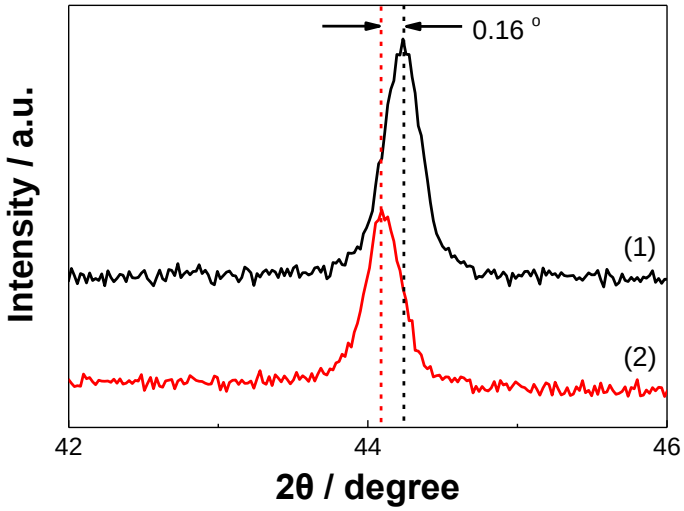

Fig. S9 XRD patterns of (1) CoCN/NG and (2) CoN+washed-NG.

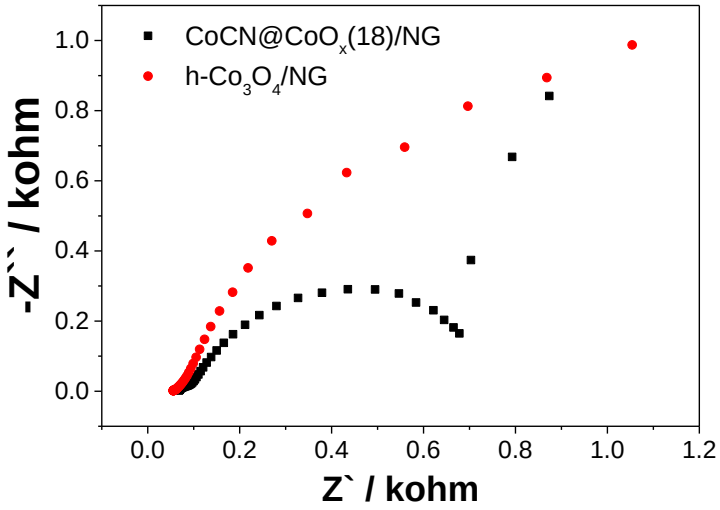

Fig. S10 EIS of CoCN@CoO_x(18)/NG and h-Co_3O_4/NG in 0.1 M KOH solution at a constant potential of -0.1 V.

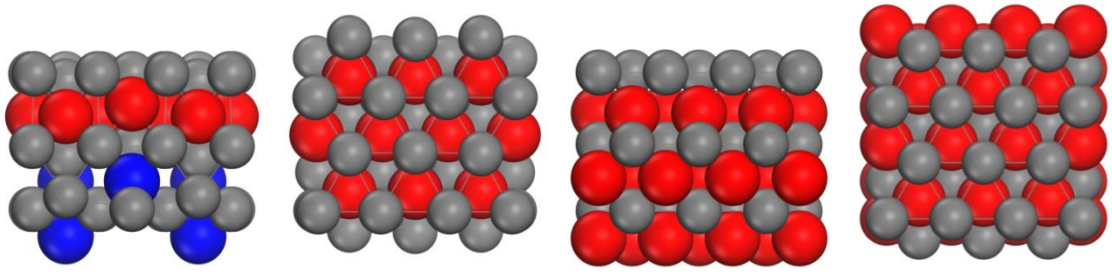

Fig. S11 CPK models of optimized structures. (a) and (b) are lateral view and vertical view of Co_4N@CoO, respectively. (c) and (d) are lateral view and vertical view of CoO, respectively. Gray: cobalt, red: oxygen, blue: nitrogen. The bond length of Co-Co on the surface in (b) is 2.430 Å, while it is 2.553 Å in (d), indicating that the interaction between cobalt atoms on the surface is stronger and the stability of the structure is enhanced when CoO wraps the Co_4N.

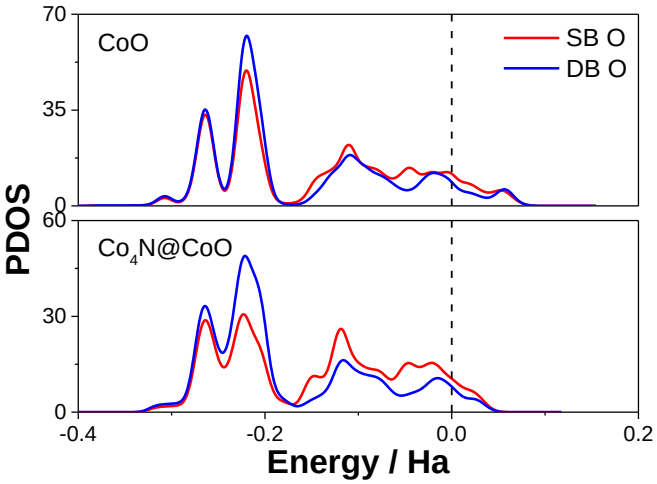

Fig. S12 PDOS of single-bonded oxygen (SB O, O 4 in Fig. 5) and double-bonded oxygen (DB O, O 5 in Fig. 5).

Table S1 Nomenclature, mass fraction of cobalt, nitrogen and oxygen and specific surface area of the catalysts.

Catalysts	Co (wt%)	N (at%)	O (at%)	S_{BET} (m^2/g)	Pore volume (cm^3/g)
CoCN@CoO_x(5)/NG	4.8	2.4	5.9	337	--
CoCN@CoO_x(18)/NG	18.0	2.4	5.1	109	0.27
CoCN@CoO_x(63)/NG	63.0	--	--	--	--
h-Co_3O_4/NG	21.3	2.3	7.3	126	0.65
NG	--	2.7	10.2	381	1.51
washed-NG	--	2.6	6.6	82	--

Table S2 Contents of three nitrogen species in various catalysts by XPS.

	N1-pyridinic N (at%)	N2-pyrrolic N (at%)	N3-graphitic N (at%)
CoCN@CoO_x(18)/NG	1.40	0.58	0.45
h-Co_3O_4/NG	1.41	0.48	0.39
NG	1.40	0.86	0.43
washed-NG	1.04	0.62	0.94

Table S3 Summary of ORR activities in 0.1 M KOH for catalysts in this work and representative catalysts in references.

Source	Materials	Half-wave potential (V vs. Ag/AgCl)	$\Delta(E_{Pt}-E_{mater.})$ at half-wave [a] (V vs. Ag/AgCl)	$J_{(-0.5V)}$ (mA cm^{-2})
This work	CoCN@CoO_x(18)/NG	-0.16	0.05	5.62

	h-Co_3O_4/NG	-0.21	0.10	4.52
2	Co_3O_4/N-rmGO	~-0.21	~0.05	~4.80
3	G-Co/CoO	~-0.18	~0.07	~4.30
4	$Co_{1-x}S$/RGO	~-0.29	--	~4.90
5	CoS_2	~-0.35	--	~3.30
6	$NiCo_2O_4$-rGO	~-0.36	~0.23	~1.38
7	$Co_{0.5}Mn_{0.5}O_yN_z$/C	~-0.29	~0.10	~4.00
8	C-COP-P-Co	~-0.24	~0.02	~5.90
9	Fe_xN/NGA	~-0.13	~0	~5.50
10	N-CG-CoO	~-0.24	--	~1.75
11	Mn_3O_4/NG	~-0.23	~0.08	~3.49
12	$La_{0.8}Sr_{0.2}MnO_3$	~-0.36	~0.16	~4.00
13	ZIF-derived N-C	~-0.34	~0.12	~3.60
14	NT-G	~-0.16	~0.01	~5.50

[a] Difference between half-wave potentials of the catalyst and Pt/C.

Table S4 Physical and geometrical properties of CoCN@CoO_x/NG catalysts.

	Co (w%)	S_{BET} (m^2/g)	D_{NPs} (nm)	D_{Core} (nm)	W_{Shell} (nm)	V_{core}/V_{shell}	Hollow (%)
CoCN@CoO_x/NG-HP	5.0	245	9.2	3.5	2.2	0.11	25.7
CoCN@CoO_x/NG-I	7.9	276	12.7	6.7	2.3	0.34	12.0
CoCN@CoO_x(5)/NG	4.8	337	14.6	9.1	2.3	0.70	10.1
CoCN@CoO_x(18)/NG	18.0	109	17.9	13.4	2.3	1.77	6.5

Table S5 Population analyses of Mulliken charge and bond length (atomic numbers refer to Fig. 5)

Substrate	Mulliken Charge (e)					Bond Length (Å)			
	1	2	3	4	5	1-4	2-5	3-5	4-5
Before adsorption									
CoO	0.088	0.088	0.088	-	-	-	-	-	-
Co_4N@CoO	0.118	0.108	0.118	-	-	-	-	-	-
After adsorption									
CoO	0.218	0.275	0.269	-0.259	-0.356	1.775	1.999	1.988	1.490
Co_4N@CoO	0.335	0.316	0.358	-0.273	-0.350	1.804	1.917	1.970	1.512

References

1. H. J. Fan, U. Gösele and M. Zacharias, *Small*, 2007, **3**, 1660-1671.
2. Y. Y. Liang, Y. G. Li, H. L. Wang, J. G. Zhou, J. Wang, T. Regier and H. J. Dai, *Nat. Mater.*, 2011, **10**, 780-786.
3. S. J. Guo, S. Zhang, L. Wu and S. H. Sun, *Angew. Chem. Int. Ed.*, 2012, **124**, 11940-11943.

4. H. Wang, Y. Liang, Y. Li and H. Dai, *Angew. Chem. Int. Ed.*, 2011, **50**, 10969-10972.
5. C. Zhao, D. Q. Li and Y. J. Feng, *J. Mater. Chem. A*, 2013, **1**, 5741-5746.
6. G. Q. Zhang, B. Y. Xia, X. Wang and X. W. Lou, *Adv. Mater.*, 2013, **26**, 2408-2412.
7. B. F. Cao, G. M. Veith, R. E. Diaz, J. Liu, E. A. Stach, R. R. Adzic and P. G. Khalifah, *Angew. Chem. Int. Ed.*, 2013, **125**, 10953-10957.
8. Z. H. Xiang, Y. H. Xue, D. P. Cao, L. Huang, J. F. Chen and L. M. Dai, *Angew. Chem. Int. Ed.*, 2014, **53**, 2433-2437.
9. H. B. Yin, C. Z. Zhang, F. Liu and Y. L. Hou, *Adv. Funct. Mater.*, 2014, **24**, 2930-2937.
10. S. Mao, Z. H. Wen, T. Z. Huang, Y. Hou and J. H. Chen, *Energy Environ. Sci.*, 2014, **7**, 609-616.
11. J. J. Duan, Y. Zheng, S. Chen, Y. H. Tang, M. Jaroniec and S. Z. Qiao, *Chem. Commun.*, 2013, **49**, 7705-7707.
12. C. Jin, X. C. Cao, L. Y. Zhang, C. Zhang and R. Z. Yang, *J. Power Sources*, 2013, **241**, 225-230.
13. P. Zhang, F. Sun, Z. H. Xiang, Z. G. Shen, J. Yun and D. P. Cao, *Energy Environ. Sci.*, 2014, **7**, 442-450.
14. Y. G. Li, W. Zhou, H. L. Wang, L. M. Xie, Y. Y. Liang, F. Wei, J.-C. Idrobo, S. J. Pennycook and H. J. Dai, *Nat. Nanotechnol.*, 2012, **7**, 394-400.